Determination of basins of attraction for SU(2) dissipative models

1988 J. Phys. A: Math. Gen. 21 2899

(http://iopscience.iop.org/0305-4470/21/13/014)

J. Phys. A: Math. Gen. 21 (1988) 2899-2909. Printed in the UK

Determination of basins of attraction for SU(2) dissipative models

E S Hernández and D M Jezek

Departmento de Física, Facultad de Ciencias Exactas y Naturales, Universidad de Buenos Aires, 1428 Buenos Aires, Argentina

Received 15 October 1987

Abstract. We propose an investigation of the properties of SU(2) non-linear Hamiltonian flows when a dissipative, gradient-like dynamics is superimposed. The corresponding flows are analysed and a method is designed to compute the boundaries of the basins of attraction to any desired accuracy. The shape and general features of these domains are examined in relation to the relative size of the dissipative component of the motion.

1. Introduction

General SU(n) models enjoy a high degree of popularity in nuclear and many-particle physics, due to their simplicity and manageability with the help of group theory techniques [1-5]. In particular, two-level models with quasispin SU(2) algebra have proven to be a useful tool for investigating aspects of the many-body problem in nuclear physics, either structural [6] or dynamical [7-12] ones. The classical phase flow of the SU(2) Hamiltonians, that appears in the frame of the mean-field or time-dependent Hartree-Fock (TDHF) theory, is a beautiful illustration of a non-linear symplectic, conservative dynamics [9-12]. However, a pure Hamiltonian view of many-particle motion cannot account for most experimental situations where macroscopic systems are involved, since in such cases it is frequently observed that small sets of quantum degrees of freedom exhibit some sort of damping in their average evolution.

With these facts in mind, we propose an investigation of the properties of SU(2) non-linear flows when a gradient dynamics is superimposed on the previous Hamiltonian motion. The phase space of the mean field or TDHF approach is the coset $S^2 = \mathrm{SU}(2)/\mathrm{U}(1)$, usually denoted as the 'Bloch sphere' [7-12]; in the presence of an extra dissipative motion, this phase space splits into basins of attraction with well defined borders [13]. The geometrical signatures of the TDHF orbits and the characteristics of the invariant regions of the SU(2) flows on S^2 permit an easy and fast visualisation of the deformed phase portrait of the dissipative evolution; furthermore, one can show that the trace of the basin border when the amount of damping is small provides an adequate indication of the shape and location of the different conservative TDHF orbits. One can additionally show that, in the case of SU(2) models plus dissipation, it is possible to compute these boundaries to any desired accuracy.

For this purpose this paper contains, in § 2, a short summary of the description of the conservative SU(2) dynamics (from the viewpoint adopted by Jezek *et al* [11, 12]) which concentrates on the motion of the quasispin vector given by a non-linear Euler

0305-4470/88/132899+11$02.50

equation. In order to include dissipation, we present, in § 3, an alternative consisting of the superposition of a gradient dynamics on the Bloch sphere S^2. In § 4 we illustrate the method for drawing the boundaries of the basins of attraction and show a sequence of figures to discuss the evolution. The conclusions are the subject of § 5.

2. The non-linear Euler equation in polarisation space

The type of motion in which we are interested consists of a gradient dissipative dynamics superimposed on a conservative TDHF motion on the Bloch sphere. The effects of dissipation will be discussed in subsequent chapters. For this purpose, in this section we briefly recall the basic formulation [11, 12] of the conservative dynamics generated by a microscopic SU(2) Hamiltonian of the form

$$\hat{H} = \boldsymbol{\Omega} \cdot \hat{\boldsymbol{J}} + \tfrac{1}{2}\alpha_{ik}\hat{J}_i\hat{J}_k \tag{2.1}$$

where J_i are the usual quasispin vector components related to fermion creation and annihilation operators, $\boldsymbol{\Omega}$ is a c vector whose z projection is the energy gap between the two single particle (SP) levels and α_{ik} is a symmetric interaction matrix. In this context, the x and y projections of the c vector $\boldsymbol{\Omega}$ represent, for example, the strengths of two external fields to which the N-particle system may couple.

The non-linear Hamiltonian flow on S^2 can be expressed by an Euler-like equation of motion for the expectation value of the quasispin operator, or polarisation vector [11, 12],

$$\dot{\boldsymbol{J}} = \boldsymbol{\Omega}^{\mathrm{HF}}(\boldsymbol{J}) \times \boldsymbol{J} \tag{2.2}$$

where $\boldsymbol{J} = \langle\tau|\hat{\boldsymbol{J}}|\tau\rangle$ is the polarisation of a Slater determinant $|\tau\rangle$ of N fermions in the two-level models [1-5] and $\boldsymbol{\Omega}^{\mathrm{HF}}(\boldsymbol{J})$ is the self-consistent frequency

$$\boldsymbol{\Omega}^{\mathrm{HF}}(\boldsymbol{J}) = \boldsymbol{\nabla}_J\langle\tau|\hat{H}|\tau\rangle. \tag{2.3}$$

Equation (2.2) is the representation of determinantal motion, or TDHF dynamics, in quasispin space and it is obtained from a variational principle [7-10]. It is useful to recall here that, due to a factorisation property of SU(2) coherent states [11], one can write the Hartree-Fock energy $\mathscr{H} = \langle\tau|H|\tau\rangle$ as a quadric in polarisation space,

$$\mathscr{H}(\boldsymbol{J}) = \boldsymbol{\Omega} \cdot \boldsymbol{J} + \tfrac{1}{2}(\chi_{ik}/J)J_iJ_k + \tfrac{1}{2}J \operatorname{Tr} \alpha \tag{2.4}$$

with

$$\chi_{ik} = (N-1)\alpha_{ik}. \tag{2.5}$$

It is then easy to compute the self-consistent frequency (2.3) that gives rise to the non-linear Euler motion described by (2.2).

3. Gradient dynamics

In this section, we present a way of introducing dissipative motion in SU(2) models. The drift of the orbit towards the local energy minimum should be provoked by a gradient-like velocity; in other words, by a component of the flow perpendicular to the equipotentials of the unperturbed motion or conservative orbits. Accordingly, in what follows we examine the modifications undergone by an SU(2) flow when a gradient-like dynamics is superimposed on the Bloch sphere. Some illustrations will be presented in § 4.

Let us now assume a modification of the geodesic flow presented in the previous section, expressed by an additive contribution to the polarisation velocity, of the type,

$$\dot{\boldsymbol{J}} = \boldsymbol{\Omega}^{\mathrm{HF}}(\boldsymbol{J}) \times \boldsymbol{J} + \boldsymbol{f}(\boldsymbol{J}) \tag{3.1}$$

where $\boldsymbol{f}(\boldsymbol{J})$ is a vector function chosen so as to satisfy the conditions:

(a) $\dot{\boldsymbol{J}} \cdot \boldsymbol{J} = 0$, i.e. the motion remains on the Bloch sphere,

(b) $\dot{\mathscr{H}}(\boldsymbol{J}) < 0$, i.e. the motion is a dissipative one,

(c) the fixed points of the flow remain invariant, and

(d) the dynamics must remain invariant under rotations in quasispin space, i.e. it should not depend upon the choice of the local coordinates.

Condition (a) requires that the vector $\boldsymbol{f}(\boldsymbol{J})$ is perpendicular to $\boldsymbol{J}$ at all times; this means the extra velocity added to the Eulerian one must be tangential to S^2. On the other hand, condition (b) can be rewritten as

$$\dot{\mathscr{H}}(\boldsymbol{J}) = \nabla_J \mathscr{H} \cdot \dot{\boldsymbol{J}} = \boldsymbol{\Omega}^{\mathrm{HF}} \cdot \dot{\boldsymbol{J}} = \boldsymbol{\Omega}^{\mathrm{HF}} \cdot \boldsymbol{f}(\boldsymbol{J}) < 0. \tag{3.2}$$

Further specification of the vector function $\boldsymbol{f}(\boldsymbol{J})$ is provided by the requirement of fixed-point invariance. This means that $\boldsymbol{f}(\boldsymbol{J}_c) = 0$, where $\boldsymbol{J}_c$ is a zero of $\boldsymbol{\Omega}^{\mathrm{HF}}(\boldsymbol{J}) \times \boldsymbol{J}$ or a Morse i-saddle of the energy function $\mathscr{H}(\boldsymbol{J})$ restricted to the Bloch sphere. Let us notice that on the two-dimensional Bloch sphere, Morse 1-saddles are usual saddle points and correspond to either

$$\boldsymbol{\Omega}_{\perp}^{\mathrm{HF}}(\boldsymbol{J}_s) = 0 \tag{3.3a}$$

or

$$\boldsymbol{\Omega}^{\mathrm{HF}}(\boldsymbol{J}_s) \| \boldsymbol{J}_s \tag{3.3b}$$

where

$$\boldsymbol{\Omega}_{\perp}^{\mathrm{HF}} = \boldsymbol{\Omega}^{\mathrm{HF}} - (\boldsymbol{J}/J^2)(\boldsymbol{\Omega}^{\mathrm{HF}} \cdot \boldsymbol{J}) = (\boldsymbol{J} \times (\nabla \mathscr{H} \times \boldsymbol{J}))/J^2 \tag{3.4}$$

is the $\nabla \mathscr{H}$ component tangential to the Bloch sphere, i.e. orthogonal to the polarisation $\boldsymbol{J}$, while Morse 0-saddles (minima) and 2-saddles (maxima) only satisfy the parallelism condition

$$\boldsymbol{\Omega}^{\mathrm{HF}}(\boldsymbol{J}_m) \| \boldsymbol{J}_m. \tag{3.5}$$

This assertion becomes clear on geometric grounds. Indeed, (3.3a) defines a two-dimensional saddle point due to the fact that $\boldsymbol{\Omega}^{\mathrm{HF}}(\boldsymbol{J})$ changes sign in a neighbourhood of $\boldsymbol{J}_s$; consequently an inversion of the Eulerian flow takes place in such a neighbourhood.

At this point it is convenient to introduce a local orthogonal (not orthonormal) coordinate system on the sphere consisting of the vectors $\boldsymbol{\Omega}^{\mathrm{HF}} \times \boldsymbol{J}$ and $\boldsymbol{\Omega}_{\perp}^{\mathrm{HF}}$. We can then express

$$\boldsymbol{f}(\boldsymbol{J}) = \alpha \boldsymbol{\Omega}^{\mathrm{HF}} \times \boldsymbol{J} + \beta \boldsymbol{\Omega}_{\perp}^{\mathrm{HF}} \tag{3.6}$$

with constant α and β, and observe that inclusion of the component parallel to the Euler velocity modifies the timescale, since (3.1) would be

$$\dot{\boldsymbol{J}} = (1+\alpha) \boldsymbol{\Omega}^{\mathrm{HF}}(\boldsymbol{J}) \times \boldsymbol{J} + \beta \boldsymbol{\Omega}_{\perp}^{\mathrm{HF}}. \tag{3.7}$$

In addition, the dissipativity condition (b) forces the parameter β to be negative. We then define a new timescale parameter $(1+\alpha)/\cos\delta$ and adopt, for convenience, the modified Euler equation

$$\dot{\boldsymbol{J}} = \cos(\delta)\boldsymbol{\Omega}^{\mathrm{HF}}(\boldsymbol{J}) \times \boldsymbol{J} - \sin(\delta)\boldsymbol{\Omega}_{\perp}^{\mathrm{HF}}(\boldsymbol{J}) \tag{3.8}$$

with $\delta = \tan^{-1}[-\beta/(1+\alpha)]$.

If δ equals zero or $\pi/2$, the motion is purely conservative or purely dissipative, respectively. Intermediate values of δ correspond to a superposition of both dynamics as indicated in (3.8).

It is now clear that this dissipative velocity vanishes at the Eulerian fixed points. More specifically, the saddle points defined in (3.3) preserve such character, since the full modified quasispin velocity in (3.1) changes sign in the vicinity of these points. Furthermore, one can realise that if the trajectory lies sufficiently close to an elliptic point (3.5), the flow velocity is the dissipative velocity $-\sin(\delta)\Omega_{\perp}^{\mathrm{HF}}(\boldsymbol{J})$ plus a linear correction,

$$\dot{\boldsymbol{J}} - \dot{\boldsymbol{J}}_{\mathrm{dis}} \approx \frac{\partial}{\partial \boldsymbol{J}}(\Omega^{\mathrm{HF}}(\boldsymbol{J}) \times \boldsymbol{J})_{\boldsymbol{J}_m}(\boldsymbol{J} - \boldsymbol{J}_m). \tag{3.9}$$

One can then visualise that flow lines near an energy minimum enter the fixed point while those near a maximum depart from it. The elliptic points then become either attractors or repulsors in the presence of the dissipative velocity; this character can be verified by performing a linear stability analysis of (3.1), where one can check after some lengthy, albeit simple, computations that the exponents are respectively negative and positive.

A few algebraic steps allow one to write the equations of motion in canonical phase space $(q_{\mathrm{HF}}, p_{\mathrm{HF}})$ [7] associated with the modified Euler equation (3.1), as follows:

$$\dot{q} = \cos(\delta)\frac{\partial \mathcal{H}}{\partial p} - \sin(\delta)\frac{1}{1-p^2}\frac{\partial \mathcal{H}}{\partial q} \tag{3.10a}$$

$$\dot{p} = -\cos(\delta)\frac{\partial \mathcal{H}}{\partial q} - \sin(\delta)(1-p^2)\frac{\partial \mathcal{H}}{\partial p}. \tag{3.10b}$$

Hereafter, we will consider a unit radius sphere, i.e. $J=1$. We then see that the dissipative component of the motion in plane phase space is 'gradient-like', however local, since the dissipation parameter is affected by positive p-dependent factors that modify the strength of the gradient components in each equation.

Furthermore, if we select an orthogonal basis of the tangent space to the (q, p) space, namely $\boldsymbol{u}_1 = (\partial\mathcal{H}/\partial p, -\partial\mathcal{H}/\partial q)$ and $\boldsymbol{u}_2 = (\partial\mathcal{H}/\partial q, \partial\mathcal{H}/\partial p)$, then equations (3.10) can be vectorially decomposed in this basis, giving

$$\begin{aligned}(\dot{q}, \dot{p}) = {} & \left[\cos\delta - \sin(\delta)\left(\frac{1}{1-p^2} - 1 + p^2\right)\frac{\partial\mathcal{H}}{\partial p}\frac{\partial\mathcal{H}}{\partial q}\frac{1}{|\boldsymbol{u}_1|^2}\right]\boldsymbol{u}_1 \\ & -\sin(\delta)\left[(1-p^2)\left(\frac{\partial\mathcal{H}}{\partial p}\right)^2 + \frac{1}{1-p^2}\left(\frac{\partial\mathcal{H}}{\partial q}\right)^2\right]\frac{1}{|\boldsymbol{u}_2|^2}\boldsymbol{u}_2.\end{aligned} \tag{3.11}$$

The apparent divergence at the poles, $p = \pm 1$ in (3.10a) is related to the impossibility of a one-to-one mapping of a sphere onto a plane.

As a final remark for this section, we point out that the modified Euler equation has been designed so as to be rotationally invariant; equation (3.11) makes it evident that the impossibility of mapping the poles onto a plane, together with the non-linearity of the coordinate transformation from the polarisation vector into canonical coordinate and momentum, gives rise to a non-gradient dynamics in plane phase space.

4. An illustration

In order to visualise the changes undergone by the TDHF flow when a gradient dynamics associated with some coordinate representation is superimposed, we have adopted a particular SU(2) Hamiltonian and computed the boundaries of the basins of attraction [13]. The Hamiltonian is the one proposed by Jezek *et al* [11], namely

$$\hat{H} = \varepsilon \hat{J}_z + \tfrac{1}{2} v \{\hat{J}_x, \hat{J}_z\} \tag{4.1}$$

where $\{\,,\}$ is the usual anticommutator. The Hamiltonian expectation value on the Bloch sphere is

$$\mathscr{H}(\boldsymbol{J}) = \varepsilon (J_z + \chi J_x J_z / J) \tag{4.2}$$

with $\chi = v(N-1)/\varepsilon$. The surfaces of constant energy in quasispin space are then hyperbolic cylinders with axis at $J_x = -J/\chi$. It has been shown [11] that as $|\chi|$ increases from zero the absolute extrema depart smoothly from the poles where they lie if $\chi = 0$, and that a non-Morse critical point appears on the intersection of the equator and the $\varphi = \pi$ meridian when $|\chi| = 1$. If $|\chi| > 1$ this point bifurcates into two saddles that separate from each other along the equator and into a relative maximum and a relative minimum that travel along the $\varphi = \pi$ meridian. Furthermore, the relative extremum of either class lies on the other side of the equator, with respect to the corresponding absolute extremum.

For a coupling constant $\chi = 1.5$ we have [11]: (i) an absolute maximum (minimum) on the plane $J_y = 0$ with $J_x > 0$ and $J_z > 0$ (<0) and (ii) a relative maximum (minimum) on the same plane with $J_x < 0$ and $J_z > 0$ (<0). The saddle points lie on the equator and correspond to the intersection between the Bloch sphere and the plane $J_x = -J/\chi$. This configuration is schematically shown in figure 1 (a more complete drawing appears in figure 4 of [11]).

It is interesting as well to comment on the effects of dissipation on the saddle eigenvectors. The dynamical system (3.11), linearised in the vicinity of the saddle

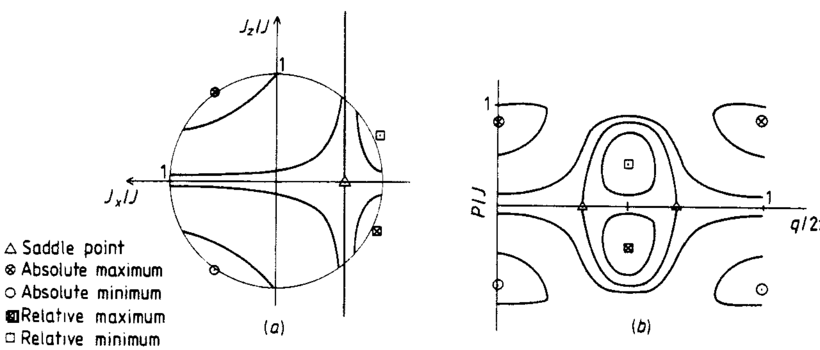

Figure 1. Orbits of the conservative flow for the Hamiltonian in (4.2) for an interaction strength $\chi = 1.5$. (*a*) Projection on the (J_x, J_z) plane of the trajectories on the Bloch sphere; (*b*) the corresponding orbits in canonical phase space. The stationary points are indicated.

point, permits a straightforward determination of the above eigenvectors and the corresponding eigenvalues, which are, in the $(q_{\rm HF}, p_{\rm HF})$ representation,

$$v_1 = \begin{pmatrix} \cos \delta/2 \\ \sin \delta/2 \end{pmatrix} \qquad \text{for} \qquad \lambda_1 = \varepsilon\chi \sin[\cos^{-1}(-1/\chi)] \tag{4.3a}$$

$$v_2 = \begin{pmatrix} \sin \delta/2 \\ -\cos \delta/2 \end{pmatrix} \qquad \text{for} \qquad \lambda_2 = -\lambda_1. \tag{4.3b}$$

We then recognise that the dissipation angle δ simply measures the rotation of the saddle eigenvectors with respect to their directions in the conservative flow, (cf figure 2) where they coincide with the axis in canonical phase space. The maximum deviation corresponds to a $\pi/4$ rotation, which is achieved in the purely dissipative case.

Since the boundaries of the basin of attraction related to each local minimum are lines connecting saddle points with nearest-lying maxima, we propose a useful numerical method to draw these lines to any desired accuracy. The procedure consists of the following steps.

(1) Locate the saddle points.

(2) Draw a line through each saddle (not on an eigenvector's direction); select one point on either half-line and evolve each of them with both the direct and the time-reversed Euler-plus dissipative dynamics as indicated in figure 2(*a*).

(3) Draw an approximate axis of the hyperbolic-like trajectories in figure 2(*a*), plot a perpendicular to the axis through the saddle, and repeat (2) as illustrated in figure 2(*b*).

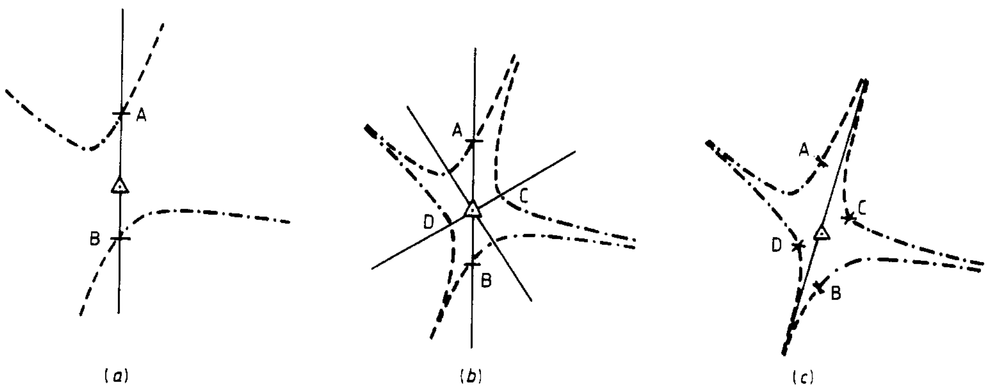

Figure 2. Schematic drawing to illustrate the method of tracing the basin borders. (*a*) Points A and B are the initial conditions. The chain curves represent the direct dynamics and the broken curves the reversed one. (*b*) Points C and D are initial conditions lying on the perpendicular to the approximate axis of the curves in (*a*). Both of them evolve as in (*a*). (*c*) The continuous line tangential to the saddle eigenvectors represents the approximate exact border within the indeterminancy region defined by the broken and chain curves. △ denotes the saddle point.

In this way one traces the borders of a closed region—which we shall refer to as the indeterminacy region (IR)—where the exact boundary is contained. If this region is small enough (in other words, if the four initial points are sufficiently close to the saddle) the reversed dynamics starting from adjacent initial conditions (in the sense of points A and C or B and D of figure 2(*b*)) provide essentially the same curve within plotter resolution. The exact border may then be reproduced by connecting through the saddle, along the eigenvector's direction, the two curves corresponding to each pair of adjacent starting points. This is illustrated in figure 2(*c*).

The method proposed here permits the IR to become as small as desired, through successive refinements of steps (1) to (3) provided that each new set of initial conditions lies inside the preceding IR. The accuracy limit imposed by this method implies a compromise with the total duration admissible for the actual computation, since the smaller the IR is, the longer each dynamics takes to drive an initial condition into its attractor.

Strictly speaking, it is not necessary that each initial condition evolves towards its corresponding attractor. However, we compute the forward evolution not only for the sake of elegance but because we feel that such a procedure possess extra advantages. On the one hand, in this way one can properly define and eventually measure the IR associated with each selection of initial conditions. On the other hand, the forward dynamics together with the reversed dynamics, permits us to draw a full orbit, whose axis can be approximately located. In this way one makes sure that the next two initial conditions can be chosen from the other side of the border as illustrated in figure 2(*b*).

Finally, we realise that if we choose another mechanism to compute these borders, the minimum number of initial conditions is not less than four, since at least two are needed to reach either of the two maxima.

The kind of figures we can obtain is displayed in figures 3-8. In each of them, part (*a*) shows the projections on the (J_x, J_z) plane of the borders of the domains on the Bloch sphere while part (*b*) shows the corresponding regions in phase space. These figures correspond to the gradient dynamics on the Bloch sphere (GDBS) for dissipation angles $\delta = \pi/2$, $3\pi/8$, $\pi/4$, $\pi/8$, $\pi/20$ and $\pi/40$. The conservative case $(\delta = 0)$ corresponds to figure 2 and the phase flow has been examined in detail by Jezek *et al* [11]. In each figure, the wider hatching indicates the basin of attraction of the relative

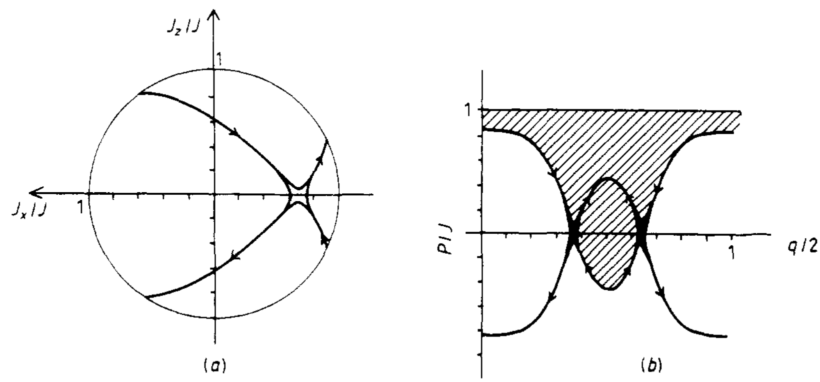

Figure 3. Basins of attraction for a dissipation strength angle $\delta = \pi/2$. (*a*) Projections on the (J_x, J_z) plane of the borders of the basins of attraction on the Bloch sphere evaluated with initial conditions on the hemisphere $J_y > 0$. (*b*) The corresponding domains in canonical phase space. The wider hatching indicates the relative minimum basin of attraction, the unshaded area is the absolute minimum basin of attraction and the closer hatching indicates the indeterminancy region. The orbits in (*b*) are computed employing initial conditions on both J_y hemispheres in order to get closed curves. The stationary points (not drawn) are the same as in figure 1. The arrows in the flow direction are drawn in order to locate the maxima and the minima in the figures; those pointing towards the saddle indicate the location of the basins' border.

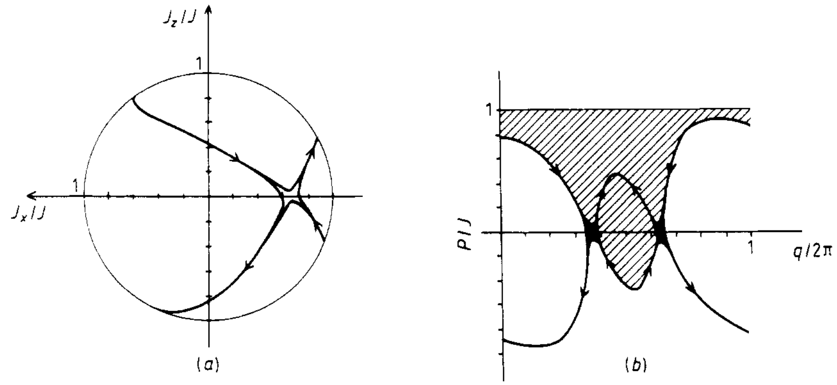

Figure 4. Same as figure 3 for $\delta = 3\pi/8$.

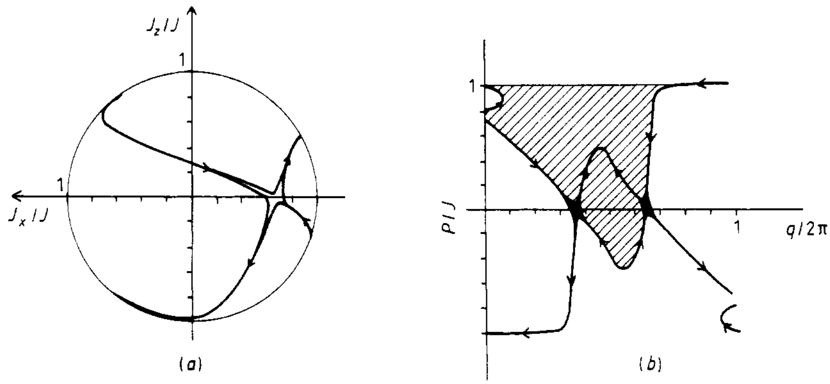

Figure 5. Same as figure 3 for $\delta = \pi/4$.

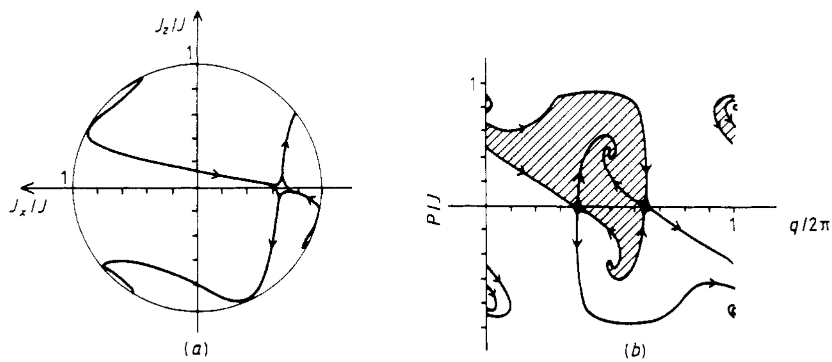

Figure 6. Same as figure 3 for $\delta = \pi/8$.

minimum, while the unshaded region corresponds to the absolute one. We also show in each figure, by closer hatching, the indeterminancy region in the neighbourhood of the saddle point inside which we have not investigated in greater detail due to computing time constraints. Actually, the basin border is the trajectory passing through the maxima; we have plotted as well, in each figure, the corresponding trajectories into

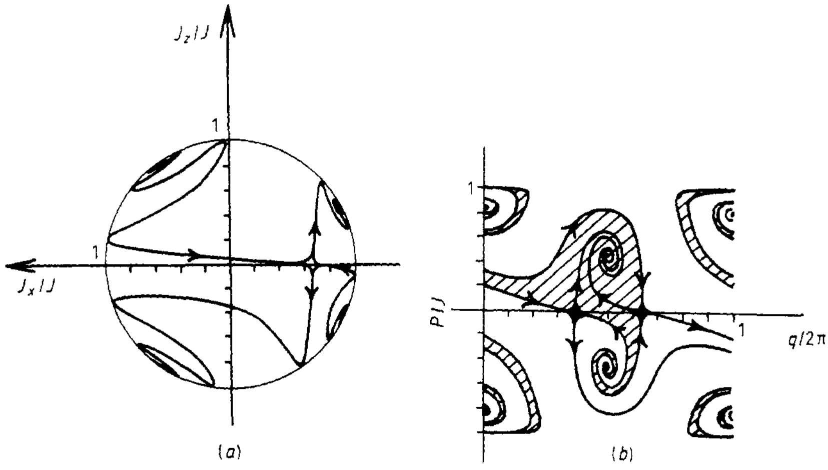

Figure 7. Same as figure 3 for $\delta = \pi/20$.

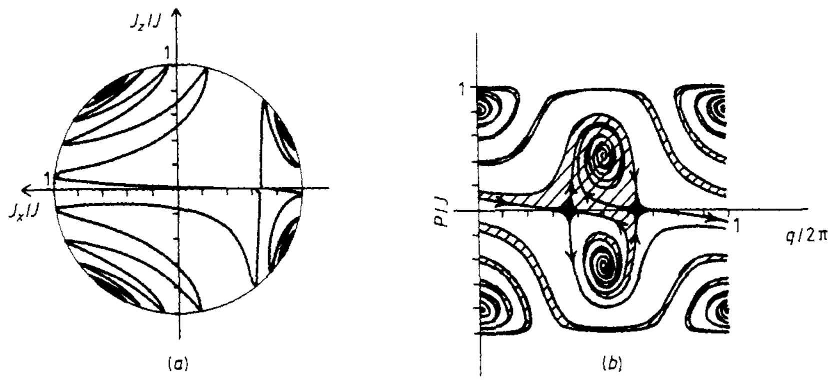

Figure 8. Same as figure 3 for $\delta = \pi/40$.

the minima computed with the forward dynamics. The latter thus illustrate the motion within each basin of attraction. Additional check-up calculations have been performed, selecting random initial conditions on S^2 and verifying the approach to the corresponding attractor, after a number of turns depending on the strength of the dissipation.

From the examination of the sequence in figures 3–8 we observe the evolution of the shape of both basins of attraction as we advance towards the purely conservative flow, starting from the purely dissipative one according to (3.8). The trend is that of a continuous deformation of each basin with increasing spiralling of the corresponding borders. In particular, figure 8 brings into evidence the almost orthogonality of the projections of the trajectories in the vicinity of the saddle point; a comparison with the purely conservative case displayed in figure 1 permits us to verify the effect of a small dissipation, namely, to locally rotate the axis corresponding to the asymptotic planes of the hyperboloid (cf (4.3)). We emphasise that such an axis rotation is actually local, since as soon as they become sufficiently far apart, the trajectories develop a larger number of turns, the smaller the dissipation, before reaching their respective attractors. These observations can be dramatically verified by reference to figure 8; it becomes clear that the borders of the basins are wildly oscillating trajectories whose arcs resemble the hyperbolic orbits of the purely conservative flow, generating in a rough and illustrative fashion all different coexistent regimes in that dynamics.

5. Summary and conclusions

In this work we have presented and analysed a possible way of transforming a conservative Hamiltonian SU(2) flow—however nonlinear, since it is generated by a Hartree-Fock Hamiltonian—into a dissipative one.

We have illustrated the conservative-plus-gradient dynamics for a choice of an SU(2) Hamiltonian whose purely conservative behaviour has been already investigated [11]. We have shown that it is possible to build up, on a numerical computation, the boundaries of the basin of attraction of each local minimum. In this situation we have analysed the evolution of these domains from pure dissipative to pure conservative motion.

The characteristic feature of the dynamics proposed here is that of a rotationally invariant flow which does not present divergences. The modified non-linear Euler equation does not depend upon local coordinates and offers the possibility of drawing a sketch of the conservative phase flow by just locating a saddle point and evolving a few points lying in a small neighbourhood. We have verified that if a low dissipation parameter is chosen, the borders of the basins of attraction indicate the position of the separatrices, the shape of the conservative orbits, the different classes of coexisting regimes and the location of the extrema.

Although the spirit of this work was to investigate the modifications undergone by the conservative non-linear Eulerian flow on the Bloch sphere in the presence of a gradient dynamics, we found it interesting to look at the phase portrait in canonical phase space $(q_{\mathrm{HF}}, p_{\mathrm{HF}})$, since the latter is traditional among nuclear theorists [7-12]. It is worthwhile recalling that there actually exist several distinct mappings (not one-to-one) of the sphere onto a plane [13]. Since the transformations among these available sets of coordinates are non-linear, it is clear that a purely dissipative dynamics imposed on given coordinates induces a conservative plus a dissipative dynamics on different representations, with coordinate-dependent coefficients and which may include some singularities (cf (3.12)).

In particular, the dissipative motion proposed by Gilmore [13] as a gradient dynamics on the set of coordinates $(x, y) = \sqrt{2}, \sin(\theta/2)\,(\cos\varphi, \sin\varphi)$, where the image of the south pole is a circle, provides an interesting example of the above remark. Indeed, one can verify that when the south pole is not a critical point (i.e. for the Hamiltonian investigated in § 4) the mapping of the conservative dynamics itself onto this flat space generates divergences in the velocity component tangential to the image circle; these are thus mapping-induced divergences. Now, as we consider the gradient dynamics, the component of $\nabla\mathscr{H}$ which provides the tangent velocity in the conservative case now gives a contribution to the radial velocity. This means that a different class of singularity may arise (i.e. dynamics-induced divergences) since as one maps the dissipative flow back onto the sphere, one obtains infinite velocities at the south pole. Such a dynamics on the Bloch sphere is a meaningless representation of any physical process undergone by N particles in a two-level system, in addition to being unacceptable on purely geometrical grounds.

Acknowledgments

The authors are indebted to the Programa de Investigaciones en Física del Plasma (PRIFIP) at their home institution for unlimited access to their computing facilities. This work was performed under Grant PID 30529 from CONICET.

References

[1] Arecchi F T, Courtens E, Gilmore R and Thomas H 1972 *Phys. Rev.* A **6** 2211
[2] Gilmore R 1972 *Ann. Phys., NY* **74** 391
[3] Gilmore R 1974 *Rev. Mex. Fis.* **23** 143
[4] Gilmore R 1977 *J. Phys. A: Math. Gen.* **10** 1131
[5] Gimore R and Feng D 1979 *Phys. Lett.* **85B** 155
[6] Lipkin H J, Meshkov H and Glick A J 1965 *Nucl. Phys.* **62** 188
[7] Kan K K, Lichtner P C, Dworzecka M and Griffin J J 1980 *Phys. Rev.* C **21** 1098
[8] Kramer P and Saraceno M 1981 *Geometry of the Time-Dependent Variational Principles in Quantum Mechanics* (Berlin: Springer)
[9] Solari H G and Hernández E S 1982 *Phys. Rev.* C **26** 2310
[10] Solari H G and Hernández E S 1983 *Phys. Rev.* C **28** 2472
[11] Jezek D M, Hernández E S and Solari H G 1986 *Phys. Rev.* C **34** 297
[12] Jezek D M and Hernández E S 1987 *Phys. Rev.* C **35** 1555
[13] Gilmore R 1981 *Catastrophe Theory for Scientists and Engineers* (Wiley: New York)